Cohesin SMC1β protects telomeres in meiocytes

Caroline Adelfalk,[1] Johannes Janschek,[1] Ekaterina Revenkova,[2] Cornelia Blei,[1] Bodo Liebe,[3] Eva Göb,[4] Manfred Alsheimer,[4] Ricardo Benavente,[4] Esther de Boer,[5] Ivana Novak,[6] Christer Höög,[6] Harry Scherthan,[3] and Rolf Jessberger[1,2]

[1]Institute of Physiological Chemistry, Medical Faculty Carl Gustav Carus, Dresden University of Technology, 01307 Dresden, Germany
[2]Department of Gene and Cell Medicine, Mount Sinai School of Medicine, New York, NY 10029
[3]Max Planck Institute of Molecular Genetics, D-14195 Berlin, Germany
[4]Department of Cell and Developmental Biology, University of Würzburg, 97074 Würzburg, Germany
[5]Memorial Sloan-Kettering Cancer Center, New York, NY 10044
[6]Department of Cell and Molecular Biology, Karolinska Institutet, S-171 77 Stockholm, Sweden

Meiosis-specific mammalian cohesin SMC1β is required for complete sister chromatid cohesion and proper axes/loop structure of axial elements (AEs) and synaptonemal complexes (SCs). During prophase I, telomeres attach to the nuclear envelope (NE), but in *Smc1β*$^{-/-}$ meiocytes, one fifth of their telomeres fail to attach. This study reveals that SMC1β serves a specific role at telomeres, which is independent of its role in determining AE/SC length and loop extension. SMC1β is necessary to prevent telomere shortening, and SMC3, present in all known cohesin complexes, properly localizes to telomeres only if SMC1β is present. Very prominently, telomeres in *Smc1β*$^{-/-}$ spermatocytes and oocytes loose their structural integrity and suffer a range of abnormalities. These include disconnection from SCs and formation of large telomeric protein–DNA extensions, extended telomere bridges between SCs, ring-like chromosomes, intrachromosomal telomeric repeats, and a reduction of SUN1 foci in the NE. We suggest that a telomere structure protected from DNA rearrangements depends on SMC1β.

Introduction

In meiosis, germ cells halve their chromosome number. Premeiotic S phase results in two pairs ("univalents") of sister chromatids, which with progression of prophase I undergo homology search, pairing to generate the "bivalent," and meiotic recombination (for reviews see Kleckner, 2006; Neale and Keeney, 2006; Costa and Cooke, 2007; Cromie and Smith, 2007; Hunt and Hassold, 2008; Vogt et al., 2008). Initially scattered throughout the nucleoplasm in premeiotic cells, the telomeres start to attach to the nuclear envelope (NE) in leptotene. Cohesins and synaptonemal complex (SC) proteins load onto the chromosomes to start forming the axial elements (AEs). With completion of leptotene, all telomeres are associated with the NE and then transiently cluster to form a structure called bouquet (Scherthan et al., 2007; for review see Siderakis and Tarsounas, 2007). In zygotene, pairing and SC formation of homologous chromosomes begins. The homologues become fully synapsed into bivalents in pachytene. During diplotene, telomeres detach from the dissolving NE, recombination proceeds, and SCs are degraded. Condensed chromosomes align on the metaphase I plate, and in anaphase I, chiasmata resolve, arm cohesion dissolves, and the homologues are separated. With completion of the second meiotic division, during which the sister chromatids are separated in a mitosis-like fashion, haploid germ cells are generated.

The mechanisms of meiotic telomere maintenance and dynamics, including attachment to the NE, are only partially understood. Telomeres are specific structures at the chromosome ends, consisting of repetitive DNA elements, TTAGGG repeats, associated with specific multisubunit protein complexes (for reviews see Blackburn, 2005; de Lange, 2005; Blasco, 2007). Double-stranded telomeric DNA transitions into an ∼150-nucleotide,

C. Adelfalk and J. Janschek contributed equally to this paper.

Correspondence to Rolf Jessberger: Rolf.Jessberger@tu-dresden.de

H. Scherthan's present address is Institut für Radiobiologie der Bundeswehr, D-80937 Munich, Germany.

Abbreviations used in this paper: AE, axial element; ALT, alternative lengthening of telomeres; chIP, chromatin IP; DIG, digoxigenin; IF, immunofluorescence; IP, immunoprecipitation; MPTA, meiotic prophase I telomere aberration; NE, nuclear envelope; SC, synaptonemal complex; telo-FISH, telomere FISH; WT, wild type.

The Rockefeller University Press $30.00
J. Cell Biol. Vol. 187 No. 2 185–199
www.jcb.org/cgi/doi/10.1083/jcb.200808016

single-stranded extension at its 3′ end, the so-called G-strand, which may form a t-loop. Telomerase, a ribonucleoprotein with reverse transcription activity, uses the G-strand 3′ end as primer for telomere repeat synthesis. Synthesis of the complementary strand by conventional DNA polymerase generates the C-strand. Most somatic cells except stem or tumor cells lack telomerase, but some telomerase activity is present in germ cells, particularly in immature, preovulation oocytes, spermatogonia, and meiosis I spermatocytes (for review see Siderakis and Tarsounas, 2007). In situ telomerase assays revealed that most telomerase activity is present during the last round of premeiotic replication, i.e., in spermatogonia (Tanemura et al., 2005). Precise assignment of telomerase-dependent telomere elongation to a specific stage in meiosis is difficult, and it is not entirely clear if, when, and how exactly telomeres are elongated during meiosis. Telomerase-independent mechanisms for telomere elongation based on homologous recombination between telomeres of different chromosomes (alternative lengthening of telomeres [ALT] pathway) may exist in meiocytes (Chin et al., 1999). In somatic cells with ALT activity, the ALT pathway generates a high degree of heterogeneity of telomeres, including elongated and shortened telomeres (for review see Nittis et al., 2008). However, this mechanism has not yet been proven to exist in germ cells.

Telomerase-deficient mice show generation-dependent and sex-specific meiosis or premeiotic phenotypes. In generation 6 (G_6) telomerase-deficient mice, premeiotic male germ cells undergo apoptosis shortly before or upon entering meiosis, whereas oocytes remain alive but produce mature oocytes with high rates of chromosomal aberrations and abnormal cell division of fertilized eggs (Hemann et al., 2001; Liu et al., 2002). In intermediate G_4 telomerase-deficient mice, the general shortening of telomeres correlates with inefficient attachment to the NE, and pachytene spermatocytes show impaired meiotic synapsis and recombination, although reduced telomere length did not always correlate with synaptic failure (Liu et al., 2004). No end to end fusions were reported in metaphase I meiocytes from G_6 telomerase-deficient mice, contrasting with the abundance of such aberrations in somatic telomerase-deficient cells. Either end fusion activities are down-regulated in meiocytes or there are meiosis-specific protection mechanisms and proteins (Siderakis and Tarsounas, 2007).

Our understanding of how telomeres are protected during meiosis is rather limited. The formation of t-loops by intrachromosomal homologous annealing of telomeric sequences may contribute to protection of telomeres, although the existence of t-loops or similar structures in meiocytes has not yet been shown. Specific telomere-binding proteins such as TRF1 and TRF2, components of the shelterin complex, containing, among others, RAP1 and Tankyrase (for review see de Lange, 2005), contribute to protection of telomeres in somatic cells. These proteins were observed at mammalian meiotic telomeres (Scherthan et al., 2000), but their functions there are not fully understood.

Telomere attachment to the NE is a hallmark of prophase I (Scherthan, 2007). Telomeres attach to the inner NE via protein complexes containing SUN domain nuclear transmembrane proteins, which link the telomeres to perinuclear motor proteins and cytoskeletal proteins (Chikashige et al., 2007; Conrad et al., 2007; Schmitt et al., 2007). In mammals, there are two such SUN domain proteins, SUN1 and SUN2. SUN2 localizes to telomere attachment sites at the NE (Schmitt et al., 2007), and deletion of SUN1 prevents telomere attachment to the NE and impairs homologue pairing and synapsis (Ding et al., 2007). After telomere attachment during the leptotene stage, the telomeres move and cluster opposite the centrosome. Thus, the chromosomes form a cluster called the bouquet, which lasts until the beginning of zygotene and is thought to promote homologous chromosome pairing, meiotic recombination, and/or subsequent metaphase plate alignment (Scherthan, 2007; de La Roche Saint-André, 2008). Toward the end of prophase I, the telomeres detach from the NE.

In mammalian cells, SMC1β cohesin is required for complete telomere attachment (Revenkova et al., 2004). In addition to proteins that form the mitotic cohesin complex (SMC1α, SMC3, Scc1/Mdc1/Rad21, Scc3/SA1, or SA2) present in somatic cells and in early prophase I meiocytes, meiocytes express several meiosis-specific components of cohesin complexes, i.e., STAG3 (homologue of SA1/SA2), REC8 (a kleisin-like Scc1), and SMC1β (in vertebrates only). SMC1β, like SMC1α, heterodimerizes with SMC3, which is the only cohesin protein found in all known cohesin complexes. SMC1β starts to appear on chromosome axes at leptotene, decorates the SC along its entire length, and disappears from chromosome arms around diplotene, but unlike SMC1α, remains on the centromeres until metaphase II (Revenkova et al., 2001). Both sexes of the *Smc1β*$^{-/-}$ mouse are infertile (Revenkova et al., 2004). Spermatocytes die at mid pachytene (stage IV/VI), whereas oocytes progress to metaphase II but accumulate single chromatids as a result of premature loss of cohesion. Phenotypes observed in *Smc1β*$^{-/-}$ meiocytes include altered chromosome axes and loop structures, impaired formation of MLH1- or MLH3-marked sites of recombination, and a failure of ∼20% of telomeres to attach to the NE (Revenkova et al., 2004; Hodges et al., 2005). Chromosome axes in *Smc1β*$^{-/-}$ meiocytes are reduced to ∼60% in length compared with wild-type (WT) cells. In contrast, chromosome axes of *Sycp3*$^{-/-}$ mice are about twice as long as WT axes (Yuan et al., 2000). Recently, we generated an *Smc1β*$^{-/-}$*Sycp3*$^{-/-}$ mouse strain to address the question how these proteins together determine chromosome architecture (Novak et al., 2008). In this double-knockout strain, axes length is mildly extended compared with WT.

Starting out with addressing the question of whether the dramatic reduction in axes length seen in *Smc1β*$^{-/-}$ spermatocytes causes the impairment in telomere attachment, we analyzed in detail the telomere phenotype of *Smc1β*$^{-/-}$ meiocytes and revealed a key role for this cohesin in protecting meiotic telomere integrity.

Results

AE/SC shortening per se does not cause failure of telomere NE attachment

Steric hindrance may occur if a minimal axis length is required for chromosomes to move both telomeres to the nuclear periphery within a certain time frame. Thus, the question emerged whether shortening of the AEs and SCs by itself causes some telomeres to fail in NE attachment in *Smc1β*$^{-/-}$ spermatocytes.

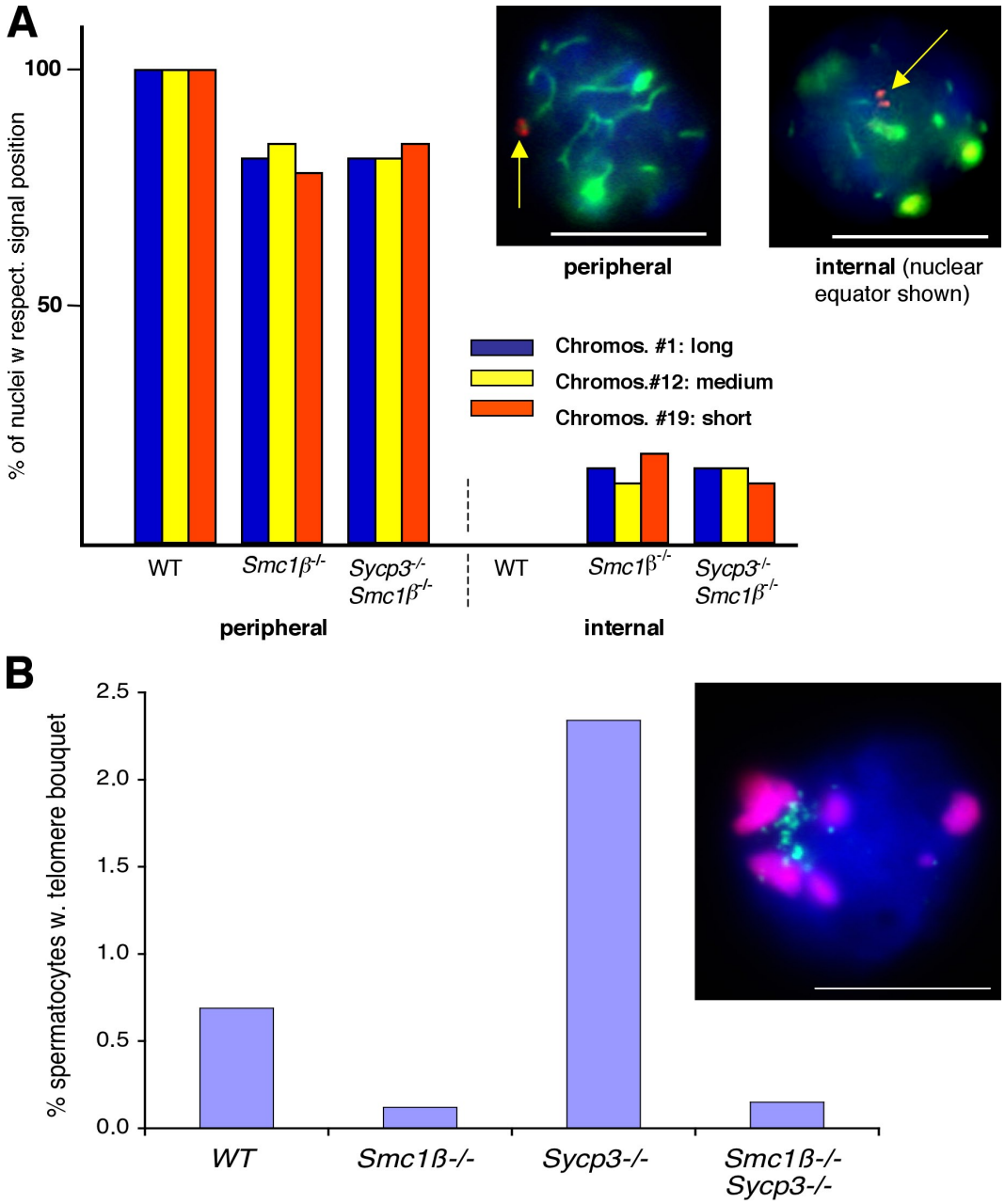

Figure 1. **Telomere clustering in spermatocytes deficient in SMC1β and SYCP3.** (A) Percentage of nuclei showing internal or peripheral position of telo-FISH signals of either chromosome No. 1 (long), 12 (medium), or 19 (short). Spermatocytes from WT, *Smc1β*$^{-/-}$, and *Smc1β*$^{-/-}$ *Sycp3*$^{-/-}$ strains were analyzed (n = 60). Examples for internal or peripheral positions are shown in the images. Red, chromosome-specific cosmid telo-FISH; green, SYCP3. The arrows point to peripheral and internal telomere signals, respectively. (B) The percentage of spermatocytes that display clustered telomeres (bouquet stage) among spermatocytes I for the mouse strains indicated (n = 4,083 [WT], 4,111 [*Smc1β*$^{-/-}$], 4,056 [*Sycp3*$^{-/-}$], and 4,019 [*Smc1β*$^{-/-}$*Sycp3*$^{-/-}$]). The inset shows an example of a bouquet staining. Green, telo-FISH; red, satellite pericentromeric major satellite probe. Bars, 10 µm.

To test this, we chose two independent approaches (Fig. 1). First, we selected three mouse chromosomes that are naturally very long (No. 1; 197 Mbp), of medium length (No. 12; 121 Mbp), or short (No. 19; 61 Mbp) and were analyzed using cosmid-based, chromosome-specific telomere FISH (telo-FISH) to determine whether they show differences in telomere attachment in either WT or *Smc1β*$^{-/-}$ spermatocytes. Second, we analyzed telomere attachment in *Smc1β*$^{-/-}$*Sycp3*$^{-/-}$ spermatocytes (Novak et al., 2008), where the AEs and remnant SCs are somewhat longer (mean of ∼18 µm) than in WT (mean of ∼12 µm), but not as long as in the *Sycp3*$^{-/-}$ strain (mean of ∼23 µm), and much longer than in the *Smc1β*$^{-/-}$ strain (mean of ∼7 µm).

Regardless of the natural length of the chosen mouse chromosomes, in *Smc1β*$^{-/-}$ spermatocytes, the same fraction (∼20%) of all three chromosomes tested localize internally, i.e., fail to attach telomeres to the NE as seen in telo-FISH staining (Fig. 1 A). Although they are longer than WT chromosomes, the same fraction of *Smc1β*$^{-/-}$*Sycp3*$^{-/-}$ chromosomes (∼20%) fails to attach telomeres to the NE (Fig. 1 A). The fraction of spermatocytes, which at a given time shows bouquet formation in

Smc1β$^{-/-}$ (0.12%) or *Smc1β*$^{-/-}$*Sycp3*$^{-/-}$ (0.15%) mice, is reduced the same to about one fifth of WT spermatocytes (0.69%; Fig. 1 B). Correcting for the pachytene arrest of *Smc1β*$^{-/-}$ spermatocytes as indicated by the absence of H1t-positive spermatocytes (Liebe et al., 2006), a significant difference was determined (P = 0.002 by χ^2 test). This contrasts with *Sycp3*$^{-/-}$ spermatocytes, which show 3.4-fold (2.34%) as many cells in the bouquet stage as WT.

From these experiments, we conclude that shortened, more compact AE/SCs and irregular loop extensions do not cause the failure of telomeres to attach to the NE in *Smc1β*$^{-/-}$ spermatocytes per se and that the *Smc1β*$^{-/-}$ telomere phenotype is dominant.

Cohesins localize to telomeres in prophase I spermatocytes

To determine whether the SMC1β protein and the SMC3 protein, the core component of the SMC1β- and SMC1α-type cohesin complexes and thus representative of all known cohesin complexes, localize to telomeres, we performed chromatin immunoprecipitation (IP [ChIP]) and immunofluorescence (IF) staining.

In *Mus musculus*, telomeres are ∼50 kbp in length (Kipling and Cooke, 1990; Starling et al., 1990). Density and distance between cohesins is highly variable, and it is unclear how many cohesin complexes to expect on telomeres. To complement IF data, which are of inherent limitations in resolution, we performed ChIP using an anti-SMC3 antibody (Fig. 2 A) and a monoclonal anti-SMC1β antibody (Fig. 2 B; Revenkova et al., 2001). Coprecipitated telomeric repeat sequences were detected by slot-blot Southern hybridization with a telomere C-strand probe.

To obtain sufficient numbers of highly purified meiosis I spermatocytes, we used a novel transgenic mouse that we recently generated, the SMC1βprom-GFP mouse (Fig. S1). In this strain, the GFP gene is expressed under the control of an SMC1β promoter region, which we have isolated. This region largely overlaps with an E2F6-binding region reported to control SMC1β expression (Storre et al., 2005). Meiocytes express GFP, starting with leptotene and increasing toward pachytene, whereafter the cells stay green into the spermatid stages (Fig. S1 A). Somatic cells, including spermatogonia, do not express GFP (Fig. S1, A–C). Thus, this mouse strain may serve as a novel meiosis indicator strain and for purification of meiocytes. In this study, we used it for FACS purification of leptotene to early pachytene spermatocytes from juvenile (day 16 postpartum) mice.

Because SMC3 is expressed in all cells unlike the meiocyte-specific SMC1β, purification of spermatocytes is particularly important as the control in anti-SMC3 ChIP. Half a million cells, >95% purity, were used per ChIP reaction. For a positive control, we used anti–histone H4 3-methylK_{20}, a heterochromatin marker known to localize to mouse pericentric regions including telomeres (Schotta et al., 2004; for review see Blasco, 2007). Anti–histone H4 3-methylK_{20} ChIP yielded a strong signal, and anti-SMC3 ChIP precipitates telomeric sequences, whereas two negative controls are blank (Fig. 2 A). For comparison in the anti-SMC3 ChIP, we also probed the precipitated material for another repetitive DNA element, SINE1B, of which about half as much telomere DNA was precipitated relative to input (Fig. S1 D). Similarly, anti-SMC1β precipitated telomere DNA from WT cells well above background seen with *Smc1β*$^{-/-}$ cells (Fig. 2 B). In anti-SMC3 ChIP from sorted GFP$^+$ WT or *Smc1β*$^{-/-}$ spermatocytes from 16-d-old mice, the telomere signal as a percentage of input was above background only in the wt samples (Fig. S1 E).

In IF experiments, we costained telomeric repeats by telo-FISH and SMC3 or SMC1β in WT or *Smc1β*$^{-/-}$ spermatocytes (Fig. 2 C). Overlapping FISH signals for telomeres and SMC3 or SMC1β were detected on WT spermatocyte chromosomes. Quantification of overlapping signals in WT and *Smc1β*$^{-/-}$ spermatocytes demonstrates more SMC3 signals without overlap and fewer with full overlap in *Smc1β*$^{-/-}$ cells. In WT cells, ∼80% of the SMC3 signals partially overlap, and ∼20% fully overlap. Only ∼5% fully overlap in *Smc1β*$^{-/-}$ cells. The nonoverlap correlates in about two thirds with gaps between the telomere and SMC3 signals. Often in WT, the SMC3–telomere overlap appears to fade shortly in front of the extreme end of the telomeres. This was also observed for colocalization of STAG3 and TRF2 in WT spermatocytes (Liebe et al., 2004). Thus, by IF, cohesin is present at least very close to the end of telomeres, but less SMC3 localizes equally close to telomeres in the absence of SMC1β. Also, we did not observe SMC3, STAG3, or SYCP3 on any of the telomere abnormalities as described for the *Smc1β*$^{-/-}$ meiocytes (see Abnormal telomere structures in the absence of SMC1β).

Ultrastructurally normal telomere attachment plates in *Smc1β*$^{-/-}$ spermatocytes

The failure of some telomeres to attach may be caused by an inability of *Smc1β*$^{-/-}$ spermatocytes to form proper attachment plates, the structures described to mediate the contact between the telomeres of the SC and the NE (Liebe et al., 2004; Schmitt et al., 2007). To ultrastructurally investigate attachment plates, attached, and nonattached SCs, we performed electron microscopy on WT or *Smc1β*$^{-/-}$ late zygotene/early pachytene spermatocyte stages (Fig. 3). Examination of *Smc1β*$^{-/-}$ spermatocytes confirmed altered chromatin compaction and a more coarse organization of chromatin fibers than in WT (Fig. 3, A–C), which is in line with previous findings (Novak et al., 2008). Nevertheless, the ultrastructures of SCs of WT and *Smc1β*$^{-/-}$ spermatocytes show no overt differences, and analysis of the attachment sites of SCs and their telomeres at the NE revealed no obvious ultrastructural differences either (Fig. 3, A and B). This was also the case for AEs of still unsynapsed chromosomes seen in *Smc1β*$^{-/-}$ pachytene meiocytes (Fig. 3 C). In *Smc1β*$^{-/-}$, but not WT cells, individual ends of SCs, marked by their centromeric heterochromatin, were occasionally observed in the nuclear interior (Fig. 3, E–E″).

We infer from this analysis that if telomeres attach in *Smc1β*$^{-/-}$ spermatocytes, the attachment plates and the attached heterochromatin and SC structures are of normal ultrastructural appearance. Also, those telomeres and adjacent SCs that were found in the nuclear interior do not display deficiencies visible by electron microscopy.

SMC1β deficiency causes reduced telomere length

To investigate structural features of telomeres in WT or *Smc1β*$^{-/-}$ spermatocytes in detail, we first determined telomere length

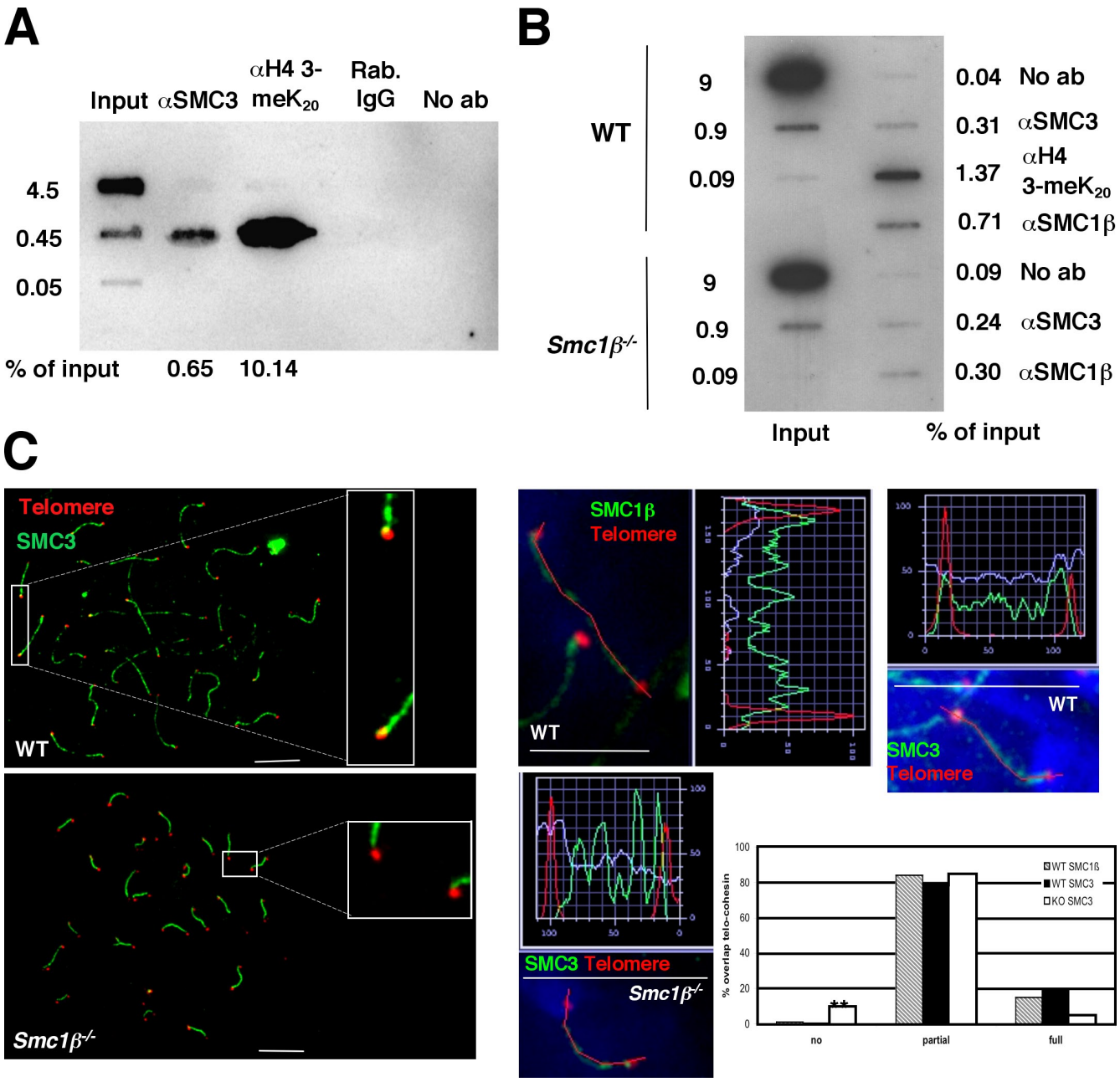

Figure 2. **SMC1β and SMC3 localization on spermatocyte telomeres.** (A) Anti-SMC3 ChIP from GFP+ spermatocytes purified by FACS from SMC1βprom-GFP juvenile mice. ChIP slot-blot analysis of telomeric DNA. Antibodies used for IP and controls (anti–H4 3-meK$_{20}$ and rabbit [Rab] IgG) are indicated. The amount of input loaded on the blot, shown as a percentage of the total, is indicated on the left. Quantification of the signals, shown as a percentage of input DNA, is shown at the bottom. (B) Anti-SMC1β or anti-SMC3 ChIP from adult WT or *Smc1β*$^{-/-}$ testis cells followed by slot-blot analysis as in A. No ab, no antibody. (C) Early pachytene spermatocyte spreads were stained with telo-FISH (red), anti-SMC3 (green), and DAPI. (left) An example of telo-FISH signals close to the SMC3-stained axis (boxed areas) are magnified in insets. (right) Quantification of SMC1β or SMC3 and telomere signals along individual chromosome axes. In WT cells, the anti-SMC1β and telo-FISH signals of the indicated chromosome (red lines) partially overlap. The marked WT chromosome stained with anti-SMC3 shows one full and one partial overlap with telomere signals. The indicated *Smc1β*$^{-/-}$ chromosome shows one telomere signal not overlapping with the SMC3 signal and one partially overlapping. The digram shows the percentage of telomere signal overlap with SMC1β or SMC3 on WT or *Smc1β*$^{-/-}$ chromosomes. *n* = 195 (WT SMC1β), 220 (WT SMC3), and 382 telomeres (KO SMC3). **, P < 0.001 by χ^2 test. Bars, 10 µM.

by two methods: (1) Southern blotting of genomic testis DNA preparations and (2) quantification of telo-FISH signals of either the G- or the C-strand of telomeres using the ImageJ software module (Fig. 4). Both methods show reduced mean telomere length in *Smc1β*$^{-/-}$ spermatocytes. In Southern blotting (Fig. 4 A, pulse field electrophoresis; and Fig. S2 A, standard gel electrophoresis), the telomere signal, typically a smear of a certain size range, is more heterogeneous with a tendency toward a lower size class than seen in WT. The extent of shortening can be very roughly estimated to be in the range of 5 kbp. However, there are still telomeres of approximately the same length as in WT. Calibrated telo-FISH image quantification confirmed shortened telomeres, for the peak fraction of telomere signal intensities

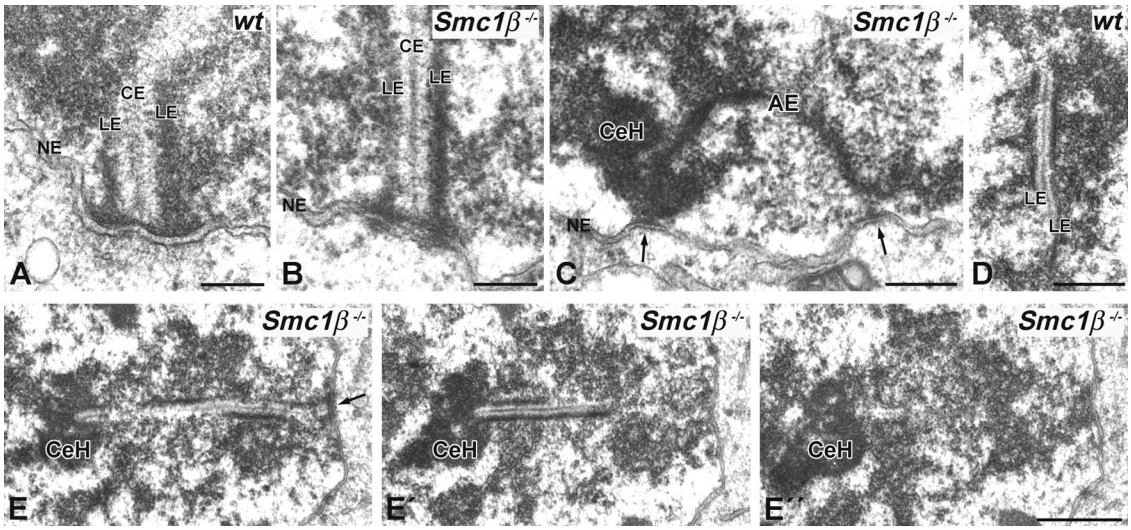

Figure 3. **Electron microscopy of telomere attachment sites in WT and *Smc1β*$^{-/-}$ mice.** (A–C) Electron-dense lateral elements (LE) of SCs (A and B) and unsynapsed AEs (C) of pachytene spermatocytes terminate with a conical thickening at the attachment plate. (C) Arrows indicate attachment sites at the NE. (D) For comparison, a WT SC is shown at the same magnification as in C. (E–E″) Three consecutive sections of a series of 12 sections through a pachytene *Smc1β*$^{-/-}$ spermatocyte showing a full-length SC. The distal telomere (lacking heterochromatin) is attached at the NE (E, arrow), whereas the proximal telomere is not associated with the NE but is free in the nuclear interior. The SC ends in the centromeric heterochromatin mass (CeH). CE, central element. Bars: (A and B) 0.2 µm; (C and D) 0.5 µm; (E–E″) 1 µm.

is shifted toward the lower intensities (Fig. 4 B). This shift increases in pachytene compared with zygotene or leptotene, as is also indicated in Fig. 4 C (box and whiskers plot). This increase in signal intensity is expected because with the completion of pairing, the signal intensity per telomere increases. These data indicate the presence of many shortened telomeres in *Smc1β*$^{-/-}$ mice. Interestingly, the distribution range of telomere length (Fig. 4 C) is almost twice as large in *Smc1β*$^{-/-}$ early pachytene spermatocytes as in corresponding WT cells, suggestive of telomere aberrations, which increase toward pachytene. In WT, the distribution range is about the same in zygotene and pachytene. The graphs in Fig. 4 B also suggest that the total number of telomeres, i.e., telo-FISH signals, in *Smc1β*$^{-/-}$ is higher than in WT spermatocytes, for the total fluorescence is higher. This was confirmed by further analysis.

One explanation for shorter telomeres would be lower levels of telomerase, which is expressed in spermatogonia and developing meiocytes, albeit at low levels (Achi et al., 2000; Riou et al., 2005). Although telomeres should be synthesized during premeiotic replication when SMC1β is not expressed, the presence of some telomerase in early spermatocytes may suggest the possibility of additional synthesis at that stage. In telomeric repeat amplification protocol assays, we detected no difference in telomerase activity in extracts from WT or *Smc1β*$^{-/-}$ testes obtained from 16-d-old mice, i.e., at an age in which WT and *Smc1β*$^{-/-}$ mice show the same testicular cellularity (unpublished data).

Abnormal telomere structures in the absence of SMC1β

Telo-FISH analysis revealed several characteristic structural aberrations of *Smc1β*$^{-/-}$ telomeres, which were either never or very rarely seen in WT spermatocytes. These abnormalities are termed meiotic prophase I telomere aberrations (MPTAs).

In early mouse meiocytes, there are 40 chromosomes with 80 telomeres visible when homologues are not paired. Ongoing homologue pairing in zygotene and pachytene stages reduces this number to ultimately 41 telomere signals, i.e., 19 perfectly paired autosomes and an XY pair that displays three signals caused by pairing of their pseudoautosomal region only. We determined a mean of ∼51 telo-FISH signals in *Smc1β*$^{-/-}$ pachytene spermatocytes (Fig. 5 A). A mean of 8.8 and 6.9 telo-FISH signals per *Smc1β*$^{-/-}$ zygotene or pachytene spermatocyte, respectively, was found without visible connection to an SC (“solitary telomeres”; Fig. 5 B). Conversely, we also observed SCs lacking telomere signals on at least one end (“telo-less SCs”; Fig. 5 C). On average, there are 3.1 telo-less SC ends per *Smc1β*$^{-/-}$ zygotene and 2.4 telo-less SCs per pachytene spermatocyte. Thus, there are approximately five excess telomere signals in mutant spermatocytes; i.e., solitary telomeres are more abundant than telo-less SCs. Very short SC fragments with a telomere signal at one end were observed in ∼77% of *Smc1β*$^{-/-}$ spermatocytes. Spatially separated telomere signals at SCs were observed in a large majority of *Smc1β*$^{-/-}$ spermatocytes (∼95%), which is indicated by split telo-FISH signals (Fig. 5 G, yellow arrow; and Fig. S4). About 23% of the cells showed one unpaired end, 64.6% showed two to six split ends (mostly two split ends), and 4.2% showed more than six (mostly seven or eight) split ends.

In almost every *Smc1β*$^{-/-}$ zygotene or early pachytene spermatocyte, we also observed telomere stretches, i.e., greatly extended fiberlike structures at the chromosome ends, which are detected by telo-FISH (Fig. 5, G [light blue arrows] and D [quantification]). These telomere stretches varied in length but reached up to 25% of the visible length of the corresponding SC. Telo-FISH staining of these stretches is often not uniform but rather appears in a dot-like pattern. In many cells (∼34%), such telomere stretches not only extend from a single SC but were found between the ends of two SCs, which is suggestive of bridging

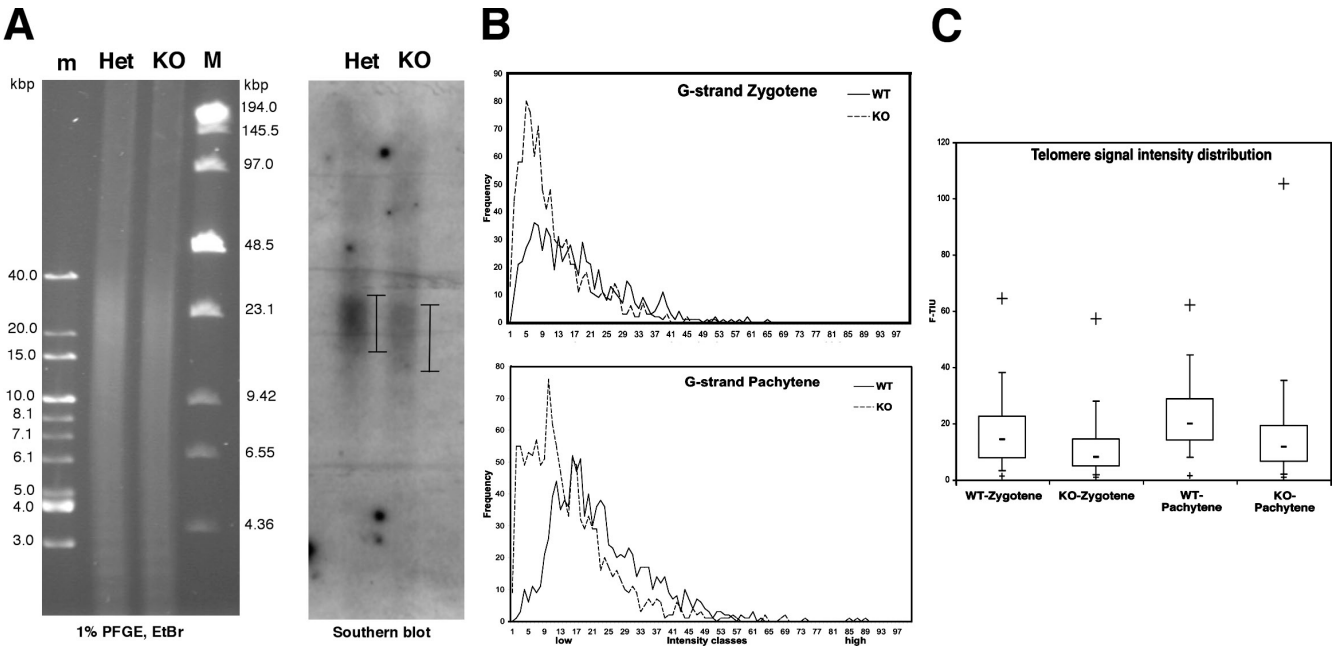

Figure 4. **Telomere length analysis.** (A) Assessment of telomere length in WT or *Smc1β*$^{-/-}$ spermatocytes. Southern blotting and ethidium bromide (EtBr)–stained gel for loading control of *Smc1β*$^{+/-}$ testis DNA (Het) and *Smc1β*$^{-/-}$ testis DNA (KO). m, DIG-labeled marker; M, pulsed field gel electrophoresis low-range marker. Bars indicate the length of the telomere signal smear. (B) Quantitative telo-FISH of zygotene or pachytene spermatocyte spreads such as those shown in Figs. 6 and 7 using ImageJ software. (C) Box and whiskers plot to visualize median lengths (−) and maximum range (+). The intervals containing the median 50% of telomere intensity values are boxed (7.8–22.5 fluorescence telomere intensity units [F-TIU]).

between telomeres. Occasionally, even ends of three or four individual SCs were apparently connected through such telomere bridges (Fig. 5 G, insets).

To test whether the telomeric aberrations observed in *Smc1β*$^{-/-}$ spermatocytes contain the G- and C-strands, we investigated all of the aforementioned MPTAs, which were probed for the G-strand, also by staining for the C-strand (Fig. S2 B). Telo-less SCs, solitary telomeres, split telomeres, telomere stretches, and telomere bridges were all seen at about the same frequency with C-strand probes as with G-strand probes.

Although solitary telomeres, telo-less SC ends, stretches, or bridges were almost never seen in WT chromosome spreads (Fig. 5, A–F), we sought to rule out the idea that the altered architecture of *Smc1β*$^{-/-}$ SCs would render them more prone to artifacts caused by spreading, albeit an unlikely possibility given our previous analysis of spread *Smc1β*$^{-/-}$ chromosomes (Revenkova et al., 2004; Hodges et al., 2005) and their confirmation in an independent SMC1β insertion mutant strain by others (Bannister and Schimenti, 2004). Nevertheless, we performed the analysis of telomere aberrations also on 3D-preserved nuclei (Fig. S3 A). Solitary telomeres, telo-less SCs, and telomere stretches were observed here as well.

A distinct, additional type of telomere aberrations, intrachromosomal telomere signals, was observed by telo-FISH in *Smc1β*$^{-/-}$ spermatocytes, albeit not at frequencies as high as the aforementioned MPTAs (Fig. 6). These telomere signals were seen either on ring-shaped (Fig. 6 A) or linear chromosomes (Fig. 6 B) at a frequency of ∼18% of *Smc1β*$^{-/-}$ spermatocytes but never in WT spermatocytes. Ring-like chromosomes and linear SCs with internal telo-FISH signals suggest chromosome rearrangements such as translocations.

Table S1 summarizes all MPTAs and their approximate frequencies. Additional examples for WT telomere stainings are provided in Fig. S3 B.

Telomere proteins localize to MPTAs

The aforementioned telomere aberrations were detected using telo-FISH and thus represent DNA structures. We next asked whether telomeric proteins are associated with these structures. We used antibodies specific for several constituents of shelterin complexes, including TRF1, TRF2, and RAP1 (Fig. 6 C; Fig. S3 B; and Fig. S4, A and B [performed on 3D-preserved nuclei]). All three proteins were found to localize to solitary telomeres, telomere stretches, and telomere bridges. Thus, the MPTAs found in *Smc1β*$^{-/-}$ spermatocytes are telomeric protein–DNA structures. RAP1 staining was occasionally observed at an end of an SC where no telo-FISH signal could be detected (Fig. S4 B). This may be an indication of very short telomere sequences that are too short to be visualized by the FISH probe but are still bound by telomeric proteins.

SUN1 association with telomeres depends on SMC1β and peripheral localization of telomeres with telomeric proteins

In mouse meiocytes, telomeres colocalize with SUN1 and SUN2 proteins throughout prophase I (Schmitt et al., 2007), and in *Sun1*$^{-/-}$ mice, telomere attachment to the NE is significantly impaired (Ding et al., 2007). In extensive IP experiments, no interaction was seen between SMC1β/SMC3 and SUN1 (unpublished data). Because telomeric proteins such as TRF1 are present on normal and aberrant telomeres of *Smc1β*$^{-/-}$ spermatocytes, we asked whether SUN1 associates with all TRF1-bearing

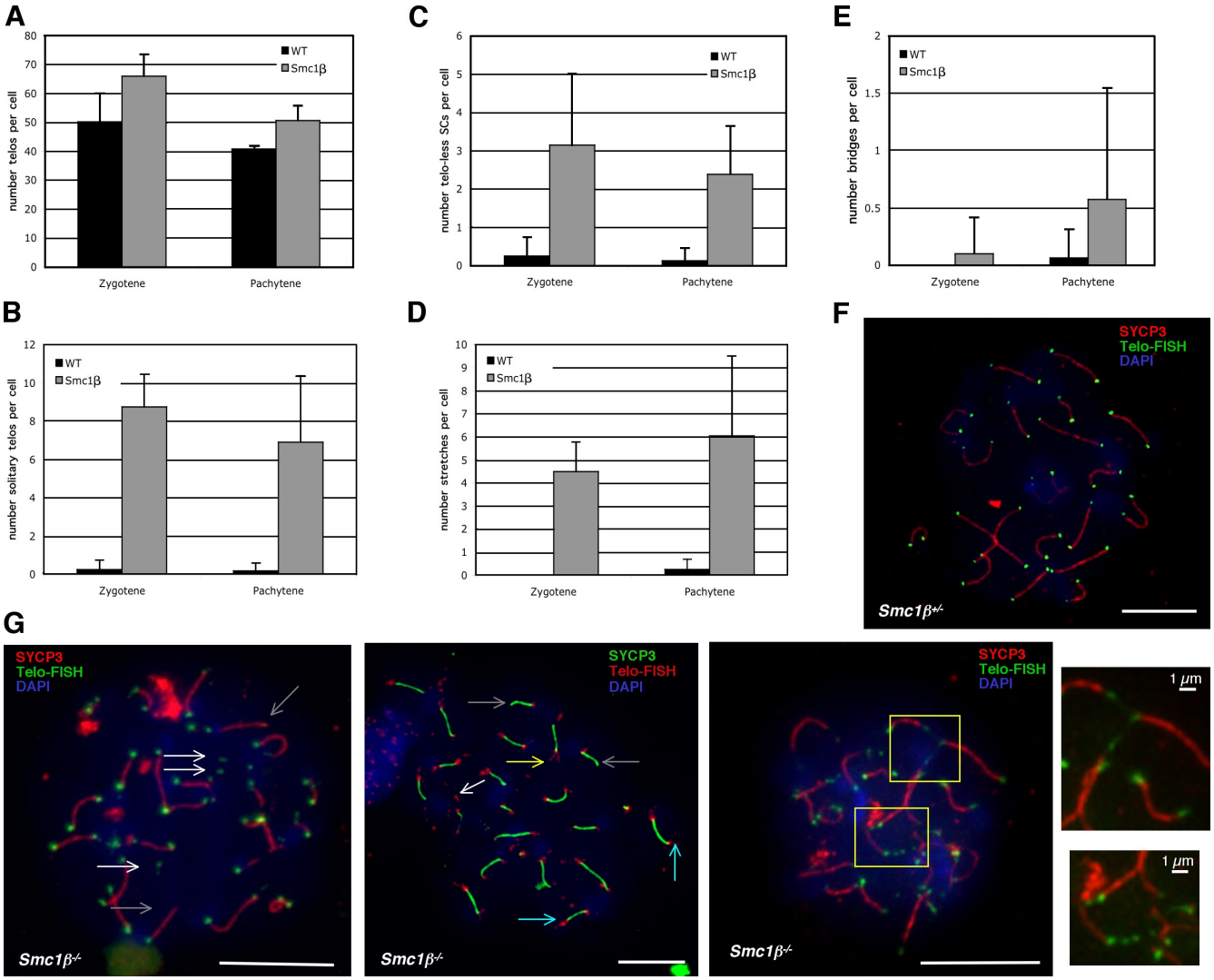

Figure 5. **Structural aberrations at chromosome ends in *Smc1β*$^{-/-}$ spermatocytes.** Analysis of G-strands by telo-FISH (green) and costaining for the SC (red, SYCP3) and DAPI of spermatocyte spreads. (A–D) Graphs show mean numbers of aberrations in WT and *Smc1β*$^{-/-}$ cells at zygotene and pachytene. (A) Total number of telomeres per cell. (B) Number of SC-less telomeres per cell. (C) Number of telo-less SCs per cell. (D) Numbers of telomere stretches per cell. (E) Number of telomere bridges per cell. Images show examples of the aberrations in *Smc1β*$^{-/-}$ pachytene cells. $P < 0.0001$. (F) *Smc1β*$^{+/-}$ pachytene cell. (G) *Smc1β*$^{-/-}$ cells. White arrows, SC-less telomeres; gray arrows, telo-less SCs; turquoise arrows, stretches; yellow arrow, unpaired telomeres. Boxed areas show apparent bridges and stretches, which are shown in higher magnification in insets. Error bars indicate SD. Bars, 10 μm (except in insets).

telomeres (Fig. 7). Costaining of the SC with TRF1 confirmed that some of the TRF1 signals are not associated with SC structures and, conversely, some SC ends are free of TRF1 signals (Fig. 7 D). Likewise, some ends appear free of SUN1, and additional SUN1 spots not visibly connected to an SC were seen (Fig. 7 E). Detailed analysis of SUN1 signals in pachytene cells showed a significantly reduced number of SUN1 spots per *Smc1β*$^{-/-}$ spermatocyte (35.89 ± 4.21) compared with WT (40.61 ± 0.59; Fig. 7 G). The number of TRF1 spots is increased (43.85 ± 2.12), which is in agreement with the aforementioned increased telo-FISH signals. Coimmunostaining for SUN1 and TRF1 (Fig. 7 F) revealed the same number of TRF1 and SUN1 spots (~41) in WT but significantly fewer SUN1 spots than TRF1 signals in *Smc1β*$^{-/-}$ spermatocytes (SUN1, 36.34 ± 4.46; TRF1, 43.97 ± 1.99). SUN1 spots always colocalized with TRF1, but there were 7.63 ± 3.97 TRF1 signals lacking SUN1. The number of such TRF1 signals (Fig. 7 G) strongly correlates with the mean number of telomeres (15–20%) that fail to attach to the NE (Fig. 1; Revenkova et al., 2004).

A further question is whether those telomeres that show structural aberrations are those that fail to attach. The high percentage of telomeres that show any kind of MPTAs (Table S1) precludes a simple correlation. Nevertheless, we analyzed the presence of aberrantly structured telomeres and altered telomere length in correlation to SUN1 spots (Fig. 8 and Fig. S5).

In *Smc1β*$^{-/-}$ spermatocytes, SUN1 signals were observed to be associated with apparently normal telomeres and with several types of MPTAs (Fig. 8, D and E; and Fig. S5, D and E). Thus, there is no correlation between structural integrity and association of telomeres with SUN1 spots, i.e., NE attachment. Telomeres overlapping with SUN1 spots often showed higher FISH signal intensity than nonoverlapping telomeres, which is indicative of more extended telomeres (Fig. 8, A and B).

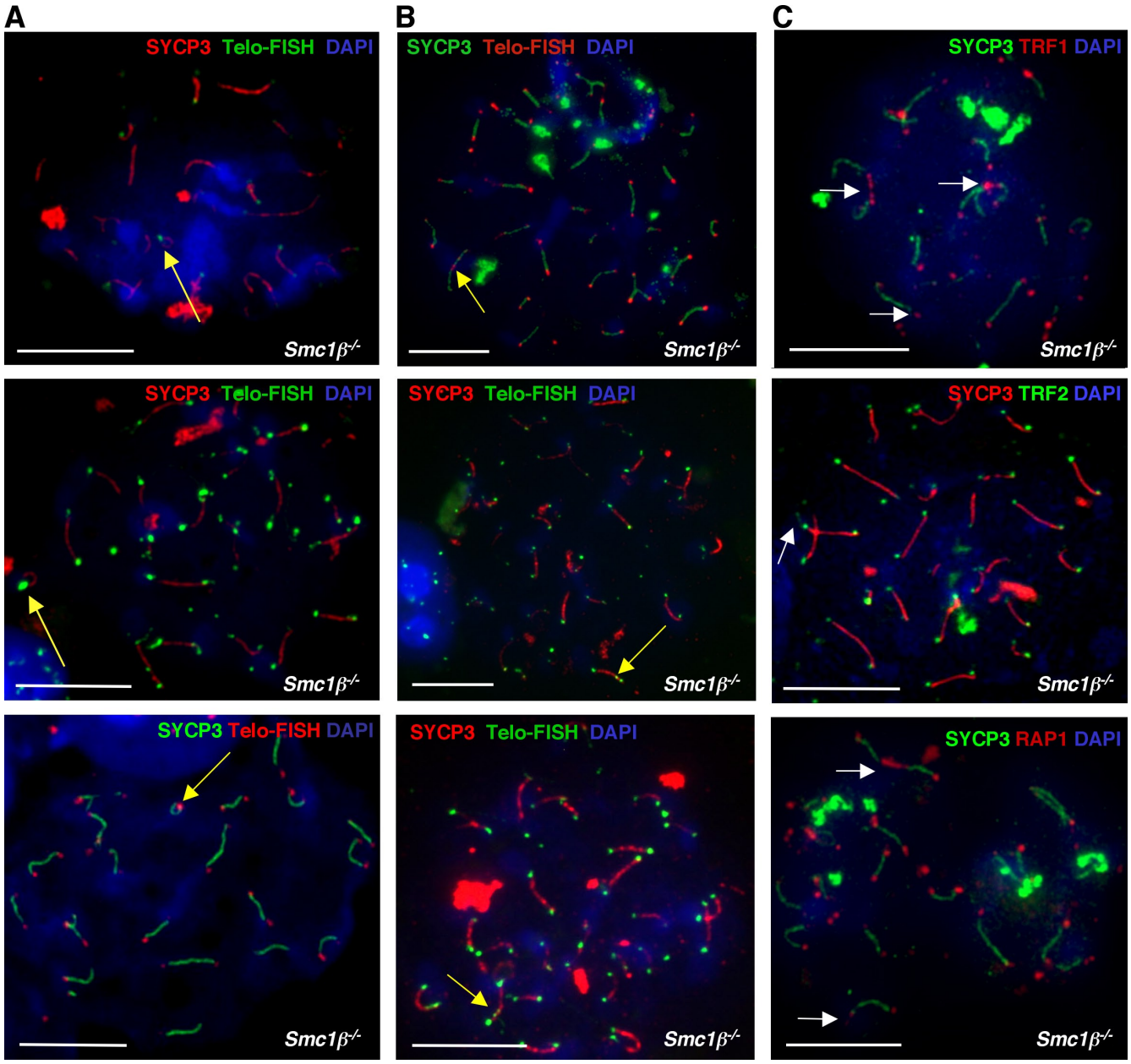

Figure 6. **Intrachromosomal telomere repeats and proteins associated with telomeric aberrations.** (A and B) Ring-like chromosomes with one telomere signal (A) and linear chromosomes with internal telomere signals (B) on the G- (green) and C-strand (red). (C) Telomere-associated proteins TRF1, TRF2, and RAP1 at telomere stretches and bridges. Bars, 10 µm. Yellow arrows point to intrachromosomal telomere signals, and white arrows indicate MPTAs associated with TRF1, TRF2, or RAP1.

Smc1β$^{-/-}$ oocytes show telomere aberrations similar to *Smc1β*$^{-/-}$ spermatocytes

Thus far, our analysis concerned spermatocytes, but *Smc1β*$^{-/-}$ oocytes also show similar general phenotypes as their male counterparts, i.e., precocious loss of cohesion, shortened axes, reduced MLH1 or MLH3 foci, and chiasmata (Revenkova et al., 2004; Hodges et al., 2005). We investigated prophase I oocyte telomeres and observed essentially the same telomere aberrations as for spermatocytes (Fig. 9). MPTAs in mutant oocytes include telo-less SCs, solitary telomeres, telomere stretches, telomere bridges, reduced telomere length, and excess numbers of telomere signals. Telomeric proteins (Rap1; Fig. 9, A and B) were also found on aberrant telomeres. None of these MPTAs were observed in WT oocytes (Fig. 9 E).

Discussion

Our initial study on reduced NE attachment of telomeres in *Smc1β*$^{-/-}$ spermatocytes (Revenkova et al., 2004) hinted at a function of the SMC1β-based cohesin complex at telomeres. As neither telomere structure and behavior nor a role for cohesins in telomere biology in mammalian meiosis are much understood, we set out to analyze the respective function of SMC1β

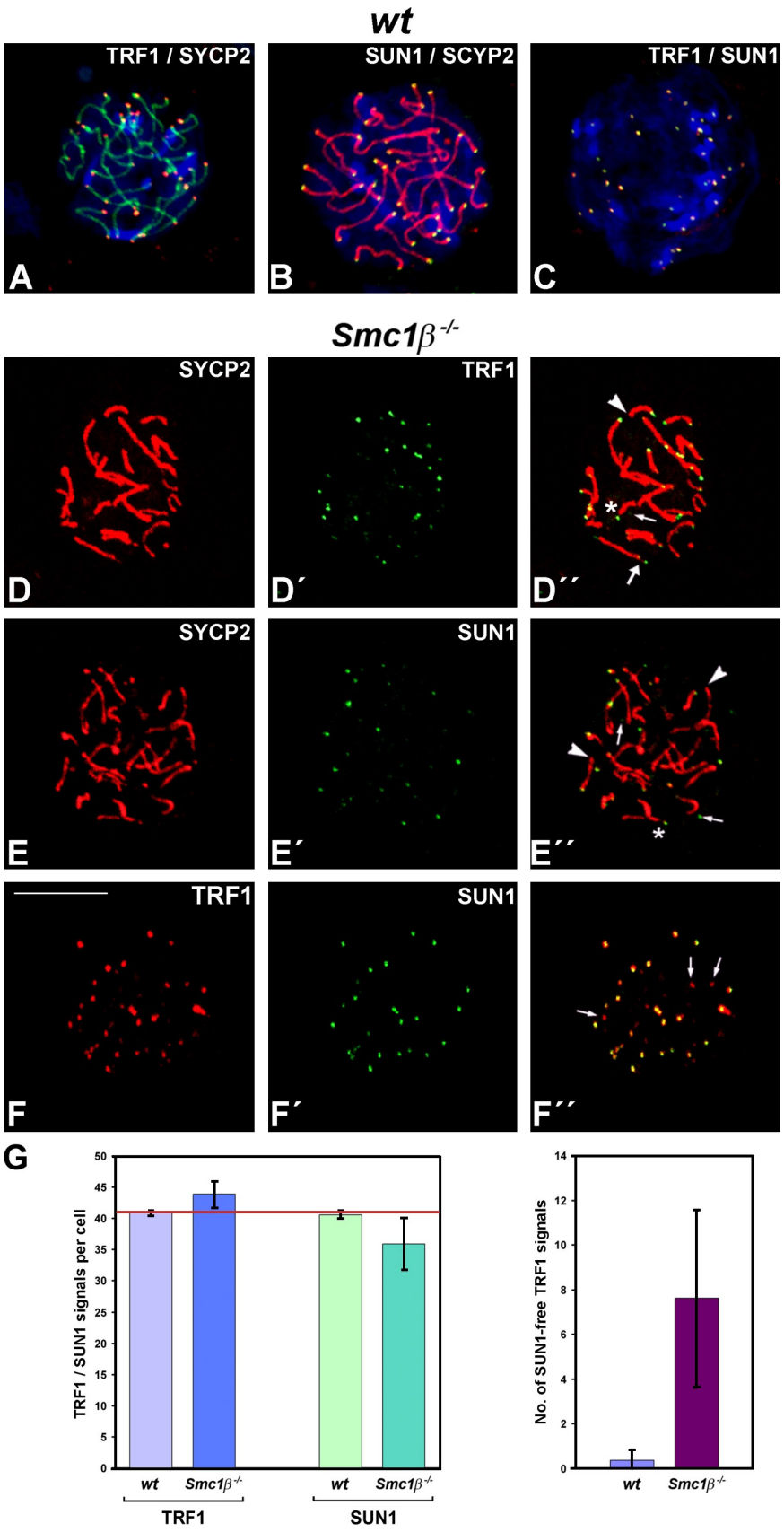

Figure 7. **Localization of SUN1 and TRF1 in WT and *Smc1β*$^{-/-}$ spermatocytes.** Images represent projections of confocal z stacks. (A–C) In WT, TRF1 (A, red), and SUN1 (B, green), both localize to the ends of the SCs (A, green; B, red) and colocalize with each other (C). (D–D″) Fluorescent images of a *Smc1β*$^{-/-}$ spermatocyte simultaneously labeled with SYCP2 (red) and TRF1 (green). The small arrow indicates TRF1 signals not associated with SC structures, and the large arrow denotes a subtelomeric unpaired and stretched AE. The arrowhead indicates an SC end without TRF1 signal. (E–E″) Simultaneous labeling with SYCP2 (red) and SUN1 (green). Ends that appear free of SUN1 are indicated by arrowheads. SC-less SUN1 spots are indicated by arrows. (D″ and E″) Asterisks indicate gaps in SCs. (F–F″) Double labeling for TRF1 (red) and SUN1 (green). Arrows indicate TRF1 signals lacking SUN1 signals. (G) Quantification of TRF1 and SUN1 signals. WT, ∼41 TRF1 (40.88 ± 0.45; $n = 42$) and SUN1 (40.61 ± 0.59; $n = 41$) spots; *Smc1β*$^{-/-}$, increased TRF1 (43.85 ± 2.12; $P < 0.001$; $n = 53$) and decreased SUN1 signals (35.89 ± 4.21; $P < 0.001$; $n = 58$). A mean of 7.63 (±3.97; $n = 32$) SUN1-less TRF1 signals are seen in *Smc1β*$^{-/-}$ (WT, 0.38 ± 0.50; $n = 21$). The red line is drawn at 41, the number of telomere signals in cells with fully synapsed chromosomes. Error bars indicate SD. Bar, 10 µm.

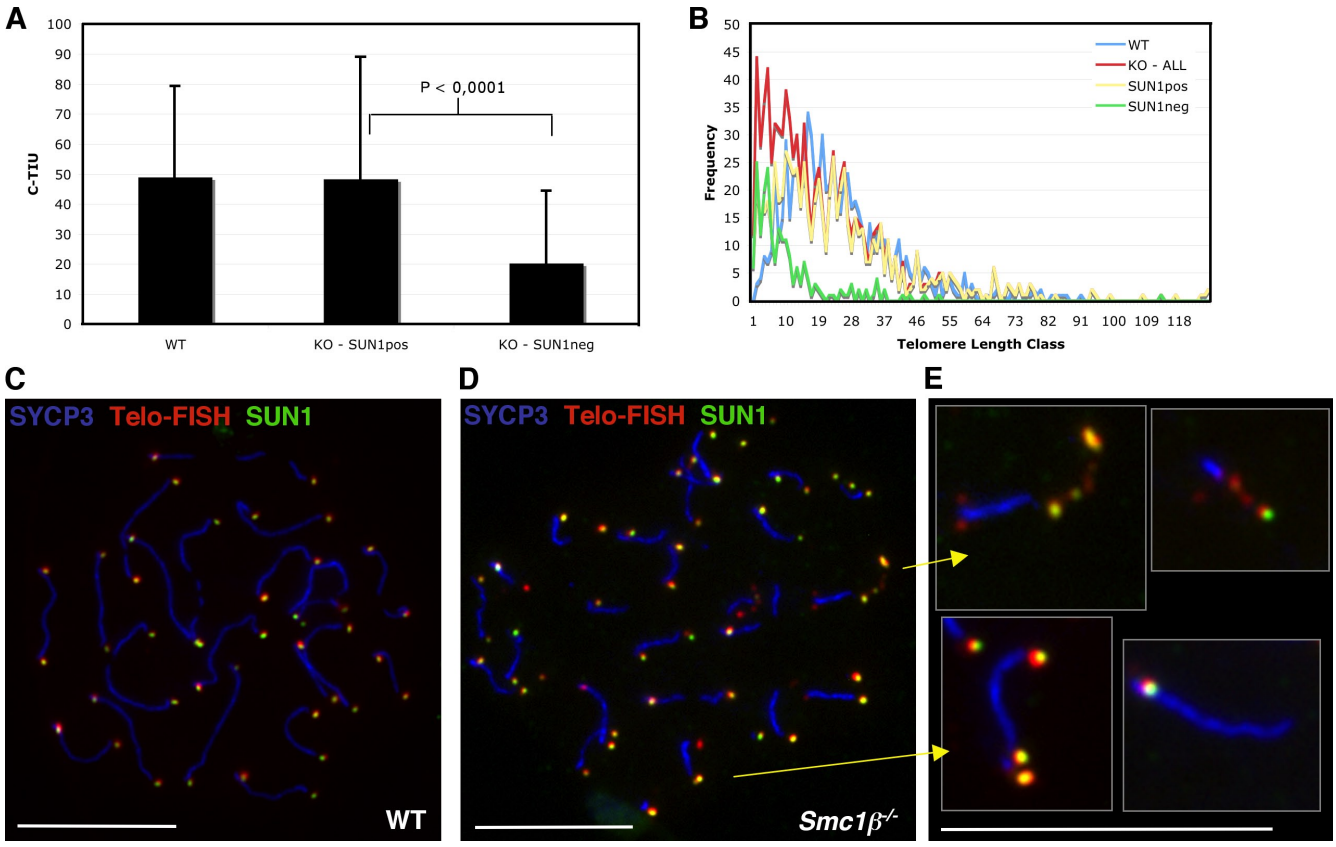

Figure 8. **Telomere aberrations and SUN1 association.** (A) Correlation of the mean telomere length as assessed by Q-FISH, i.e., telomere signal intensity with presence or absence of SUN1. In WT, all telomeres are associated with SUN1. (B) Distribution of telomere length and association with SUN1 (SUN1pos and SUN1neg) for *Smc1β*$^{-/-}$ pachytene spermatocytes; the WT distribution of telomere length is shown for comparison. (C–E) Telo-FISH combined with IF staining for SYCP3 and SUN1 in WT (C) and *Smc1β*$^{-/-}$ spermatocytes (D and E). (E) Individual aberrant telomere structures from D as indicated (arrows) or from similar images. Error bars indicate SD. Bars, 10 μm.

in detail. The data presented in this study prove that SMC1β has a genuine, specific function at meiotic telomeres.

The main findings are that SMC1β is required (1) to support NE attachment independently of AE and SC length and of the presence of the AE protein SYCP3, (2) to properly localize cohesin complexes at telomeres, (3) to preserve telomere length, (4) to maintain structural integrity of telomeres, which in absence of SMC1β show a plethora of different types and qualities of MPTAs (5) for complete SUN1 protein colocalization with telomeres. We also show that (6) telomere aberrations, except shortening, do not correlate with SUN1 association and thus attachment failure and that (7) SMC1β fulfills its function at telomeres in both spermatocytes and oocytes.

The telomere phenotypes described in this study are not a consequence of apoptosis of *Smc1β*$^{-/-}$ meiocytes because the phenotypes appear much earlier (starting in leptotene stage and increasing in zygotene stage) than entry of spermatocytes into apoptosis at early to mid pachytene stage, and there is no appreciable apoptosis in leptotene to pachytene oocytes. Apoptosis triggered by a premeiotic checkpoint, as reported by Liu et al. (2004), is not relevant because SMC1β is only expressed after the initiation of meiosis. The telomere phenotypes are also not a consequence of impaired meiotic recombination and chiasmata formation because the early events in meiotic recombination such as Rad51 foci formation are not affected by SMC1β deficiency (Revenkova et al., 2004), and only events starting in pachytene stage with MLH foci formation and later chiasma formation and maintenance are impaired. The reverse, an effect of telomere deficiencies on spermatocyte survival or recombination in spermatocytes and oocytes, can currently neither be excluded nor proven. A putative spermatocyte telomere attachment checkpoint shall be investigated in the future.

In the absence of SMC1β, ∼15–20% of telomeres fail to attach to the NE, which correlates with decreased SUN1 foci at the NE, indicating that SUN1 foci formation depends on proper interaction of telomeres with the NE. However, there is no correlation of telomere structural integrity and SUN1 association because SUN1 was observed to localize to both normal and aberrant telomeres. Because the resolution of microscopy techniques is limited, one cannot exclude that in *Smc1β*$^{-/-}$ meiocytes, all telomeres are aberrant, some with very minor structural aberrations. Given the high percentage of visible MPTAs, this does not seem unlikely. One can also not exclude that a few of the MPTAs are caused by the failure to attach and thus are indirect. However, given the lack of correlation, the contribution of this mechanism, if it exists, should be minor.

In somatic cells, the cohesin subunit SA-1 associates with TRF1 (Canudas et al., 2007), and in maize, afd1 (Rec8) alleles affect telomere bouquet formation (Golubovskaya et al., 2006). The presence of cohesin and SC proteins at meiotic subtelomeric

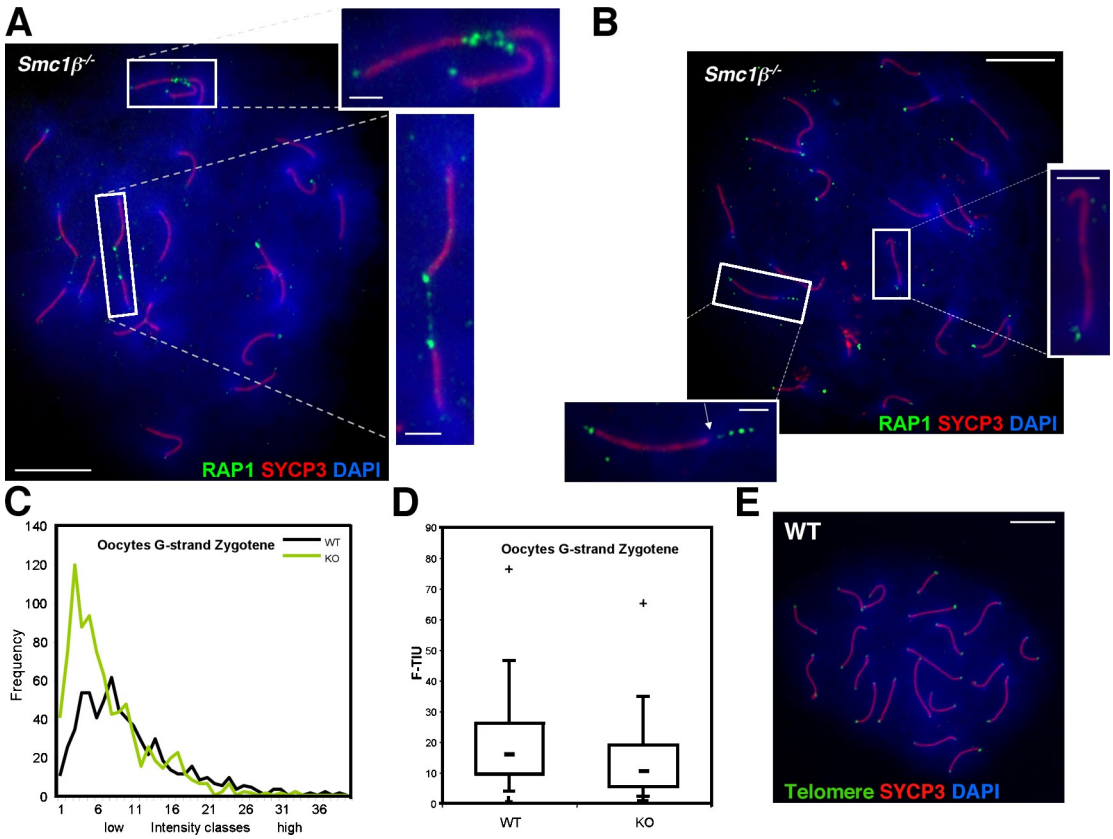

Figure 9. **MPTAs in *Smc1β*$^{-/-}$ oocytes.** (A and B) IF images showing a variety of aberrations in pachytene oocytes. (A) Telomere bridges visualized by RAP1 staining (green) between two or three SCs (SYCP3, red). (B) Gaps (arrow) between the telomeric signal (RAP1, green) and the SC (SYCP3, red; left inset), and split telomeres at one end and no telomere signal on the other end of a chromosome (right inset). (C and D) Quantification of telomere length of zygotene oocytes (n = 10 each). (C) Intensity plot of the telomere signal gained by G-strand telo-FISH. (D) Whisker box plot of WT and *Smc1β*$^{-/-}$ (KO) cells showing the median telomere length (−) and the maximum length range (+). (E) WT oocyte control staining. Insets indicate individual chromosome magnifications of the indicated boxed areas. Bars: (whole nucleus images) 10 µm; (insets) 2 µm.

and telomeric regions was shown previously for STAG3 and SYCP2 (Liebe et al., 2004) and is shown in this study for SMC1β and for SMC3, which is core component of all known cohesin complexes. IF signals for SMC1β or SMC3 do not completely overlap with telo-FISH signals at the extreme end of the telomeres. Considering the limitations in resolution, this left somewhat uncertain whether SMC1β and SMC3 indeed bind telomere repeat DNA in prophase I spermatocytes, which we therefore showed by ChIP from FACS-purified spermatocytes I or total testis cells. Interestingly, less SMC3 IF staining at telomeres was detected in *Smc1β*$^{-/-}$ spermatocyte spreads. Because all other regions of meiotic chromosomes continue to show staining for SMC3 and other cohesins (Revenkova et al., 2004), this does not reflect a general failure of SMC3 to associate with AEs or SCs in the absence of SMC1β, but rather, it reflects a telomere-specific deficiency. This also indicates that other cohesins, including SMC1α-type complexes, do not prominently localize to telomeres either because they all require SMC3. Thus, in meiosis, the SMC1β-type cohesin complex is the prevalent cohesin complex present at telomeres.

There are several putative mechanisms that may cause telomere abnormalities in the absence of SMC1β. These mechanisms are only briefly mentioned, as they remain speculative and are secondary to unprotection through loss of SMC1β.

We disproved the initial hypothesis for the attachment failure to be a consequence of the drastic shortening of the prophase I chromosomal axes and irregular extension of chromatin loops by comparison of naturally short or long chromosomes and by the analysis of the *Sycp3*$^{-/-}$*Smc1β*$^{-/-}$ double mutant. The *Smc1β*$^{-/-}$ phenotype is dominant, strongly suggesting a specific role for SMC1β at telomeres.

The asynapsis observed in some *Smc1β*$^{-/-}$ meiocytes (at least 30% of spermatocytes and 10% of oocytes; Revenkova et al., 2004; Novak et al., 2008) is not likely a major cause for the MPTAs because at least one MPTA is present in every meiocyte (Table S1). There are many solitary telomeres, telo-less SCs, stretches, and bridges in *Smc1β*$^{-/-}$ meiocytes, and thus, the increased numbers of telo-FISH signals cannot result only from the occasional unpaired telomeres of otherwise normal SCs. There is no apparent correlation between asynapsed or partially synapsed chromosomes and the occurrence of MPTAs. Nevertheless, one cannot rigorously exclude that delays in synapsis, partial synapsis, or asynapsis contribute to formation of some MPTAs because unprotected telomeres may be more prone to aberrations if asynapsed. However, thus far, telomere phenotypes were not reported in other mutant mouse strains that display asynapsis.

Reduction in mean telomere length and an extended range of length classes as well as the large variety of structural MPTAs

suggest that in the absence of SMC1β, telomeres are unprotected and may therefore be prone to recombination processes. Because SMC1β is not expressed during premeiotic replication, replication-associated processes are unlikely. ALT-like pathways may be triggered, although IF staining for promyelocytic leukemia bodies did not reveal any difference between WT and *Smc1β*$^{-/-}$ cells (unpublished data). Internal telomeric sequences clearly indicate DNA rearrangements in the absence of SMC1β, e.g., nonhomologous end joining between a telomere linked to an SC fragment and a telomere or unequal homologous recombination between stretches of homology on different chromosomes. Telo-FISH signals lacking SC signals and vice versa indicate breakage of telomeric regions from SCs. Often, telomeric sequences were observed that are linked to a small remnant of an SC, likely another breakage product. The increase in the distribution range of telomere length from leptotene to pachytene stage can thus be explained through continuous unequal exchange processes.

Protein–DNA bridges may result from fusion of telomeric ends of sister chromatids of one homologue or of two pairs of still unpaired homologues. This can be seen in cells with chromosome core numbers >20 and where the two cores linked by a bridge are of the same length. In most cases, however, the bridges connect nonhomologous chromosomes, often fully synapsed bivalents with each four sister chromatids. The occasional appearance of bridges that connect three SCs further underscores this point. G-strands may become extended upon deprotection and may anneal with complementary strands of another chromosome or may form Hogsteen G–G base pairs with another G-strand and thus form noncovalent bridges between telomeres, possibly explaining the stretches.

Collectively, we suggest that SMC1β serves to protect telomere structure. The maintenance of telomere structure and length may be necessary for complete NE attachment. Because reduced telomere length is known to cause attachment failures (Liu et al., 2004), we suggest that attachment failure and length reduction are events secondary to unprotection. It is clear from the data presented in this study that once SMC1β is lost, meiotic telomeres suffer a large variety of abnormalities, MPTAs. One can currently only speculate about the mechanism of protection. Considering the ability of cohesin to embrace two sister chromatids and thus hold them in close proximity (Gruber et al., 2003) and the binding of structural maintenance of chromosomes protein domains to unusual DNA structures such as stem loops (Akhmedov et al., 1999), it seems possible that cohesin supports or even forms special DNA structures at the very end of chromosomes. Whether they are t-loops that are stabilized by cohesin binding or other structures, such as terminal DNA loops, with the very end looped back and clamped without strand invasion and thus fixed to a more interior region is unknown. However, we propose that SMC1β cohesin is required for a protective telomere architecture.

Materials and methods

Mice

Derivation of the *Smc1β*$^{-/-}$, *Sycp3*$^{-/-}$, and *Smc1β*$^{-/-}$*Sycp3*$^{-/-}$ knockout mice has been previously described (Yuan et al., 2000; Revenkova et al., 2004; Novak et al., 2008).

To generate the Smc1βprom-GFP mice, we PCR amplified a fragment of mouse *Smc1β* promoter located between positions −283 and −12 from the translation start codon and inserted it between the AseI and AgeI sites of pEGFP-C1 (Takara Bio Inc.). The linearized plasmid was microinjected into the pronuclei of fertilized eggs of B6C3 F1 hybrid mice. The eggs gave rise to several SMC1βprom-GFP founder mice. Cell suspensions from spleen, lung, kidney, liver, and testis obtained by digestion with Liberase (Roche) were analyzed by fluorescence-activated cell sorting for GFP expression as described previously (Vasileva et al., 2006). Mice were genotyped by tail DNA PCR. To detect pregnancy, females were caged with males, and the vaginal plugs were examined every morning. The day when the plug was found was marked as embryonic day (E) 0.5. For prophase I ovary sampling, pregnant female mice were sacrificed at E16.5. To collect ovaries of postnatal stages, the pups were sacrificed at day 1 after birth (1 d postpartum).

Testicular and ovarian preparations

Testis suspensions yielding structurally preserved nuclei for simultaneous SC immunostaining and FISH were prepared as described previously (Liebe et al., 2004). In brief, a testicular cell suspension was mixed with fixative solution (3.7% formaldehyde and 0.1 M sucrose) in equal volumes on a glass slide. The mixture was spread over the slide and was allowed to dry at 4°C.

Detergent spreading of spermatocytes was modified from studies described previously (Peters et al., 1997; Scherthan et al., 2000; Peters and Meister, 2007) and performed as follows: ∼10 µl of a testicular suspension was placed on a glass slide and mixed gently with 80 µl ionic detergent solution 1% Lipsol (LIP Equipment, Inc.). After 10 min, cells were mixed with 1% PFA, 5 mM $NaBH_3$, pH 9.2, and 0.15% Triton X-100 and were let to dry in a humid chamber for 2 h. Thereafter, slides were washed four times with 1% Agepon (Agfa Inc.), dried at RT, and kept at −80°C until use. Oocyte spreading was performed in a similar way (Peters et al., 1997). Ovaries were incubated for 15 min in a hypotonic buffer (30 mM Tris, pH 8.2, 50 mM sucrose, 17 mM Na-citrate, 5 mM EDTA, and 0.5 mM DTT) placed under a stereomicroscope (Stemi 1000 or 2000-C with cold light epi-illumination KL 1500 LCD; Carl Zeiss, Inc.) on a glass slide and punched with needles in 100 mM sucrose solution to release the oocytes. After a 5-min incubation in a wet chamber, an equal amount of 2% PFA, pH 9.2, and 0.3% Triton X-100 was added. Slides were left to dry in the wet chamber for 1.5 h and were washed four times with 1% Agepon. Slides were stored at −80°C. 3D-preserved cells were prepared by adding an equal volume of 3.7% formaldehyde and 0.1 M sucrose in PBS to cell suspensions on a slide and drying them at 4°C.

For histological analysis of the SMC1βprom-GFP mice, testes were punctured with a 22-gauge needle and fixed in phosphate-buffered formalin, pH 7.4, and embedded in cold-polymerizing methacrylate resin (Technovit 8100; Heraeus Kulzer GmbH) according to the manufacturer's instructions. 2-µm adjacent sections were analyzed by fluorescence and light microscopy. For light microscopy, sections were stained with hematoxylin and eosin.

IF

Immunolabeling was performed as described previously (Roig et al., 2004). Slides with spread or 3D-preserved cells were incubated with primary antibodies at 4°C overnight and secondary antibodies for 45–60 min at 37°C. When combining telo-FISH with IF, biotinylated secondary antibodies against primary rabbit or mouse antibodies (Genetex Inc.) were used. Those were detected by FITC-, Cy3-, or AMCA (7-amino-4-methyl-coumarin-3–acetic acid)-conjugated avidin or streptavidin and incubated for 30 min at 37°C. Primary antibodies used were rabbit polyclonal anti-SYCP3 and mouse monoclonal anti-SYCP3 (provided by C. Heyting, Wageningen University, Wageningen, Netherlands), rabbit polyclonal anti-SMC3 (Eijpe et al., 2000), rabbit polyclonal anti-SMC1β raised against the N terminus and rabbit polyclonal anti-STAG3 (Revenkova et al., 2004), rabbit polyclonal anti-TRF1 and rabbit polyclonal anti-RAP1 (provided by T. de Lange, The Rockefeller University, New York, NY), rabbit polyclonal anti-TRF1 (#2-S; Alpha Diagnostic), rabbit polyclonal anti-TRF2 (Novus Biologicals), affinity-purified guinea pig and rabbit polyclonal anti-SYCP2, which were raised against amino acids 1,089–1,505 of mouse SYCP2, and affinity-purified guniea pig anti-SUN1 (raised against a peptide corresponding to amino acids 428–722 of murine SUN1). The following secondary antibodies were used: Cy2-, Cy3-, Cy5-, Texas red–, or biotin-conjugated goat anti–rabbit (Jackson ImmunoResearch Laboratories, Inc.), FITC-conjugated goat anti–rabbit (SouthernBiotech), FITC-conjugated mouse anti–rabbit, biotin-conjugated donkey anti–mouse, and Cy2- or Texas red–conjugated goat anti–guinea pig (Jackson ImmunoResearch Laboratories, Inc.). Slides were mounted with mounting medium (Vectashield; Vector Laboratories).

Microscopic evaluation

Preparations were evaluated using an epifluorescence microscope (AxioPhot or Axioskop; Carl Zeiss, Inc.) equipped with single-band pass filters for excitation of green, red, blue, and infrared and Plan Neofluar 63×/1.25 NA, Plan Apochromat 100×/1.4 NA, and Plan Neofluar 100×/1.30 NA oil immersion lenses (Carl Zeiss, Inc.). Images were recorded at RT with a camera (AxioCam MRm; Carl Zeiss, Inc.) using AxioVision software (version 4.4; Carl Zeiss, Inc.) or the ISIS fluorescence image analysis system (MetaSystems). Images were further processed using Paint Shop Pro (Corel) or Photoshop (CS2; Adobe) to match the fluorescence intensity seen in the microscope. 3D evaluations were performed using confocal microscopy systems (LSM 510 [Carl Zeiss, Inc.] or TCS-SP2 AOBS [Leica]). Imaging was performed using a Plan Apochromat 63×/1.4 NA oil differential interference contrast objective. Lasers 405, 488, 561, and 633 nm were used for excitation of DAPI, FITC, Texas red, and Cy2, Cy3, or Cy5, respectively. Images were acquired using the corresponding LSM software packages.

Immuno-FISH procedures

Immunostaining was combined with FISH, and the slides were denatured in 70% deionized formamide/2× SSC at 70°C for 4 min and hybridized with chromosome-specific probes (denaturation of the probe at 75°C for 10 min) for 40 h at 37°C as described previously (Liebe et al., 2004). The telomere-specific BAC probes were selected from Korenberg et al. (1999). They were specific to ends of chromosomes Nos. 1 (45C1; proximal end), 12 (34I19; distal end), 18 (51B23; distal end), and 19 (26B5 proximal; 49P14; distal end) and directly labeled with DIG11-dUTP by nick translation (Roche). After hybridization, washes and detection were performed as described previously (Liebe et al., 2004). After FISH, slides were incubated with the respective SYCP3 antibodies and detected by anti–rabbit FITC antibodies (Jackson ImmunoResearch Laboratories, Inc.).

Electron microscopy

Testes were fixed in 2.5% cacodylate-buffered glutaraldehyde (for 1 h at 4°C) and postfixed with 1% osmium tetroxide (for 1 h). After overnight staining with 0.5% uranyl acetate, testes were dehydrated in ethanol series and embedded in epon. Ultrathin sections were double stained with uranyl acetate and lead citrate. Micrographs were obtained with an electron microscope (EM-10; Carl Zeiss, Inc.).

Telomere length assays

A testis cell suspension was made as described previously (Bastos et al., 2005). In brief, the tubules were digested by collagenase in DME (Invitrogen) two times for 25 min at 32°C. The cells were washed twice and used for DNA isolation. Cells were incubated for 3 h at 55°C in lysis buffer (10 mM Tris-HCl, pH 8.0, 10 mM EDTA, 100 mM NaCl, 40 mM DTT, 2% SDS, and 20 µg/ml proteinase K; 10^6 cells/µl buffer), and DNA was isolated by phenol/chloroform/isoamylalcohol (25:24:1) extraction. 1 µg DNA for standard gel electrophoresis or 11.5 µg DNA for pulse field gel electrophoresis was used per sample and digested with HinfI and RsaI at 37°C for 2 h. Samples were loaded together with a digoxigenin (DIG)-labeled broad-range marker (Invitrogen; labeled with DIG nucleotides [Roche] using T4 polymerase) on a 0.8% agarose gel or with a low-range pulsed field gel electrophoresis marker (New England Biolabs, Inc.) on a 1.0% pulse field–certified agarose (Bio-Rad Laboratories) gel. Blotting was performed overnight in RT. Transferred DNA was cross-linked to the membrane with UV light. Membrane was hybridized overnight either with a ^{32}P-labeled A(CCCTAA)$_{12}$ oligonucleotide or a DIG-labeled telomere probe (Roche) at 42°C. Alkaline phosphatase–conjugated anti-DIG antibodies were used for detection, and the light signal that was recorded by an image station (2000R; Kodak) using image analysis software (1D; Kodak). Telo-FISH of the G-strand was performed using the Telomere PNA FISH/FITC kit (Dako). For the C-strand, a Cy3-conjugated telomere PNA probe (Panagene) was used. The hybridization occurred for 3 h at RT after a denaturation at 80°C for 5 min. Cells from WT and *Smc1β*$^{-/-}$ mice from the same litter were always hybridized at the same time and compared with each other. The relative length of telomeres was estimated by measuring the fluorescence intensity using ImageJ (National Institutes of Health) with the zwi reader plugin. The background was subtracted as a value of 20, and the threshold was set to 150. For calibration of the FISH signals, we used fluorescent-labeled microbeads (0.5 µm; Invitrogen). Calibration was performed at regular time intervals (30 min) during each microscopy session. Two grayscale images of beads were recorded for each slide/image, and a mean value was calculated and used as a calibration standard.

Telomerase activity assays

The telomeric repeat amplification protocol assay was performed using the TRAPeze XL Telomerase Detection kit (Millipore) following the manufacturer's instructions. Whole ovaries or testes were minced. Oocytes were isolated by punching them out of embryonic ovaries, and spermatocytes were FACS sorted using SMC1βprom-GFP mice. Tissues or cells were lysed in CHAPS lysis buffer on ice and kept at −80°C until all samples were collected. The Bradford assay was performed to measure protein concentration. 500 ng of protein from each sample was used for the reaction. Negative controls of each sample were made by heat inactivation at 85°C for 10 min. The first step of the reaction is an extension of a TS primer by the telomerase occurring at 30°C for 30 min. The resulting products are amplified in a PCR reaction at 94°C for 30 s, at 59°C for 30 s, and at 72°C for 1 min, repeated for 45 cycles. A last incubation step occurs at 55°C for 25 min. PCR products were separated on a 10% nondenaturing polyacrylamide gel and stained with ethidium bromide.

ChIP

For some ChIP experiments, we sorted GFP-positive cells from 16-d-old SMC1βprom-GFP mice using a cell sorter (Influx; Cytopeia, Inc.) and Spigot software (version 5.3.8) or a FACSAria II and the Diva software (BD). For one IP, we used 5×10^5 cells. Where total testis cells were used, 2×10^6 cells were used. ChIP was performed as described previously (García-Cao et al., 2004). The following antibodies were used: 5 µg rabbit polyclonal antibody to SMC3 (Bethyl Laboratories, Inc. or self-made; Eijpe et al., 2000), 5 µg mouse monoclonal anti-SMC1β (clone #70; IgG2a), 2.5 µg rabbit polyclonal antibody to histone H4 (trimethyl K20; Abcam), 5 µg rabbit IgG (Santa Cruz Biotechnology, Inc.), or no antibody. After phenol chloroform extraction, DNA fragments were precipitated with ethanol in the presence of 10 µg/ml glycogen, slot blotted onto Hybond N+ membrane (GE Healthcare), and hybridized with ^{32}P-labeled C-strand oligonucleotide A(CCCTAA)$_{12}$ overnight at 60°C. We quantified the signals using PhosphorImager (Molecular Dynamics) or ImageJ.

Statistics

Statistics were performed using the Student's *t* test (http://www.graphpad.com/quickcalcs/ttest1.cfm), by box whiskers plot calculations (WinSTAT; Excel; Microsoft), or by χ^2 test (http://www.daten-consult.de).

Online supplemental material

Fig. S1 shows a testis section from an SMC1βprom-GFP mouse and FACS sorting of meiotic cells from this mouse strain. Such cells were used for ChIP experiments. Fig. S2 shows the altered telomeres in *Smc1β*$^{-/-}$ spermatocytes by Southern blotting probed with a telomere probe. Diagrams show the frequencies of different MPTAs for the telomeric C-strand. Fig. S3 shows MPTAs in a 3D-preserved *Smc1β*$^{-/-}$ spermatocyte stained with anti-SYCP3 and telo-FISH and examples of spread WT spermatocytes with different stainings. Fig. S4 shows MPTAs in 3D-preserved *Smc1β*$^{-/-}$ spermatocytes stained with TRF2, RAP1, and telo-FISH. Fig. S5 shows TRF1 and SUN1 localization in WT and *Smc1β*$^{-/-}$ spermatocytes. Frequencies of MPTAs in spermatocytes and oocytes are listed in Table S1. Online supplemental material is available at http://www.jcb.org/cgi/content/full/jcb.200808016/DC1.

We thank Drs. Attila Toth, Evelin Schröck, and Ursula Eichenlaub-Ritter for critical reading and discussing the manuscript and Drs. Titia de Lange and Christa Heyting for antibodies.

This work was supported by the Deutsche Forschungsgemeinschaft (grants JE150/4-1, SPP1384, and JE150/10-1 to R. Jessberger, grant Al 1090/1-1 to M. Alsheimer, and grant Be 1168/6-3 to R. Benavente) and the National Institutes of Health (grant R01GM062517 to R. Jessberger and E. Revenkova). R. Benavente was supported the Graduate School Organogenesis. H. Scherthan was supported by H.H. Ropers (Max-Planck Institute for Molecular Genetics, Berlin, Germany). C. Höög was supported by the Swedish Cancer Society, the Swedish Research Council, and the Karolinska Institute.

Submitted: 5 August 2008
Accepted: 17 September 2009

References

Achi, M.V., N. Ravindranath, and M. Dym. 2000. Telomere length in male germ cells is inversely correlated with telomerase activity. *Biol. Reprod.* 63:591–598. doi:10.1095/biolreprod63.2.591

Akhmedov, A.T., B. Gross, and R. Jessberger. 1999. Mammalian SMC3 C-terminal and coiled-coil protein domains specifically bind palindromic

DNA, do not block DNA ends, and prevent DNA bending. *J. Biol. Chem.* 274:38216–38224. doi:10.1074/jbc.274.53.38216

Bannister, L.A., and J.C. Schimenti. 2004. Homologous recombinational repair proteins in mouse meiosis. *Cytogenet. Genome Res.* 107:191–200. doi:10.1159/000080597

Bastos, H., B. Lassalle, A. Chicheportiche, L. Riou, J. Testart, I. Allemand, and P. Fouchet. 2005. Flow cytometric characterization of viable meiotic and postmeiotic cells by Hoechst 33342 in mouse spermatogenesis. *Cytometry A.* 65:40–49.

Blackburn, E.H. 2005. Telomeres and telomerase: their mechanisms of action and the effects of altering their functions. *FEBS Lett.* 579:859–862. doi:10.1016/j.febslet.2004.11.036

Blasco, M.A. 2007. The epigenetic regulation of mammalian telomeres. *Nat. Rev. Genet.* 8:299–309. doi:10.1038/nrg2047

Canudas, S., B.R. Houghtaling, J.Y. Kim, J.N. Dynek, W.G. Chang, and S. Smith. 2007. Protein requirements for sister telomere association in human cells. *EMBO J.* 26:4867–4878. doi:10.1038/sj.emboj.7601903

Chikashige, Y., T. Haraguchi, and Y. Hiraoka. 2007. Another way to move chromosomes. *Chromosoma.* 116:497–505. doi:10.1007/s00412-007-0114-8

Chin, L., S.E. Artandi, Q. Shen, A. Tam, S.L. Lee, G.J. Gottlieb, C.W. Greider, and R.A. DePinho. 1999. p53 deficiency rescues the adverse effects of telomere loss and cooperates with telomere dysfunction to accelerate carcinogenesis. *Cell.* 97:527–538. doi:10.1016/S0092-8674(00)80762-X

Conrad, M.N., C.-Y. Lee, J.L. Wilkerson, and M.E. Dresser. 2007. MPS3 mediates meiotic bouquet formation in *Saccharomyces cerevisiae*. *Proc. Natl. Acad. Sci. USA.* 104:8863–8868. doi:10.1073/pnas.0606165104

Costa, Y., and H.J. Cooke. 2007. Dissecting the mammalian synaptonemal complex using targeted mutations. *Chromosome Res.* 15:579–589. doi:10.1007/s10577-007-1142-1

Cromie, G.A., and G.R. Smith. 2007. Branching out: meiotic recombination and its regulation. *Trends Cell Biol.* 17:448–455. doi:10.1016/j.tcb.2007.07.007

de La Roche Saint-André, C. 2008. Alternative ends: telomeres and meiosis. *Biochimie.* 90:181–189. doi:10.1016/j.biochi.2007.08.010

de Lange, T. 2005. Shelterin: the protein complex that shapes and safeguards human telomeres. *Genes Dev.* 19:2100–2110. doi:10.1101/gad.1346005

Ding, X., R. Xu, J. Yu, T. Xu, Y. Zhuang, and M. Han. 2007. SUN1 is required for telomere attachment to nuclear envelope and gametogenesis in mice. *Dev. Cell.* 12:863–872. doi:10.1016/j.devcel.2007.03.018

Eijpe, M., C. Heyting, B. Gross, and R. Jessberger. 2000. Association of mammalian SMC1 and SMC3 proteins with meiotic chromosomes and synaptonemal complexes. *J. Cell Sci.* 113:673–682.

García-Cao, M., R. O'Sullivan, A.H. Peters, T. Jenuwein, and M.A. Blasco. 2004. Epigenetic regulation of telomere length in mammalian cells by the Suv39h1 and Suv39h2 histone methyltransferases. *Nat. Genet.* 36:94–99. doi:10.1038/ng1278

Golubovskaya, I.N., O. Hamant, L. Timofejeva, C.J. Wang, D. Braun, R. Meeley, and W.Z. Cande. 2006. Alleles of afd1 dissect REC8 functions during meiotic prophase I. *J. Cell Sci.* 119:3306–3315. doi:10.1242/jcs.03054

Gruber, S., C.H. Haering, and K. Nasmyth. 2003. Chromosomal cohesin forms a ring. *Cell.* 112:765–777. doi:10.1016/S0092-8674(03)00162-4

Hemann, M.T., K.L. Rudolph, M.A. Strong, R.A. DePinho, L. Chin, and C.W. Greider. 2001. Telomere dysfunction triggers developmentally regulated germ cell apoptosis. *Mol. Biol. Cell.* 12:2023–2030.

Hodges, C.A., E. Revenkova, R. Jessberger, T.J. Hassold, and P.A. Hunt. 2005. SMC1beta-deficient female mice provide evidence that cohesins are a missing link in age-related nondisjunction. *Nat. Genet.* 37:1351–1355. doi:10.1038/ng1672

Hunt, P.A., and T.J. Hassold. 2008. Human female meiosis: what makes a good egg go bad? *Trends Genet.* 24:86–93. doi:10.1016/j.tig.2007.11.010

Kipling, D., and H.J. Cooke. 1990. Hypervariable ultra-long telomeres in mice. *Nature.* 347:400–402. doi:10.1038/347400a0

Kleckner, N. 2006. Chiasma formation: chromatin/axis interplay and the role(s) of the synaptonemal complex. *Chromosoma.* 115:175–194. doi:10.1007/s00412-006-0055-7

Korenberg, J.R., X.N. Chen, K.L. Devon, D. Noya, M.L. Oster-Granite, and B.W. Birren. 1999. Mouse molecular cytogenetic resource: 157 BACs link the chromosomal and genetic maps. *Genome Res.* 9:514–523. doi:10.1101/gr.9.10.994

Liebe, B., M. Alsheimer, C. Höög, R. Benavente, and H. Scherthan. 2004. Telomere attachment, meiotic chromosome condensation, pairing, and bouquet stage duration are modified in spermatocytes lacking axial elements. *Mol. Biol. Cell.* 15:827–837. doi:10.1091/mbc.E03-07-0524

Liebe, B., G. Petukhova, M. Barchi, M. Bellani, H. Braselmann, T. Nakano, T.K. Pandita, M. Jasin, A. Fornace, M.L. Meistrich, et al. 2006. Mutations that affect meiosis in male mice influence the dynamics of the mid-preleptotene and bouquet stages. *Exp. Cell Res.* 312:3768–3781. doi:10.1016/j.yexcr.2006.07.019

Liu, L., M. Blasco, J. Trimarchi, and D. Keefe. 2002. An essential role for functional telomeres in mouse germ cells during fertilization and early development. *Dev. Biol.* 249:74–84. doi:10.1006/dbio.2002.0735

Liu, L., S. Franco, B. Spyropoulos, P.B. Moens, M.A. Blasco, and D.L. Keefe. 2004. Irregular telomeres impair meiotic synapsis and recombination in mice. *Proc. Natl. Acad. Sci. USA.* 101:6496–6501. doi:10.1073/pnas.0400755101

Neale, M.J., and S. Keeney. 2006. Clarifying the mechanics of DNA strand exchange in meiotic recombination. *Nature.* 442:153–158. doi:10.1038/nature04885

Nittis, T., L. Guittat, and S.A. Stewart. 2008. Alternative lengthening of telomeres (ALT) and chromatin: is there a connection? *Biochimie.* 90:5–12. doi:10.1016/j.biochi.2007.08.009

Novak, I., H. Wang, E. Revenkova, R. Jessberger, H. Scherthan, and C. Höög. 2008. Cohesin Smc1β determines meiotic chromatin axis loop organization. *J. Cell Biol.* 180:83–90. doi:10.1083/jcb.200706136

Peters, L., and G. Meister. 2007. Argonaute proteins: mediators of RNA silencing. *Mol. Cell.* 26:611–623. doi:10.1016/j.molcel.2007.05.001

Peters, A.H., A.W. Plug, M.J. van Vugt, and P. de Boer. 1997. A drying-down technique for the spreading of mammalian meiocytes from the male and female germline. *Chromosome Res.* 5:66–68. doi:10.1023/A:1018445520117

Revenkova, E., M. Eijpe, C. Heyting, B. Gross, and R. Jessberger. 2001. Novel meiosis-specific isoform of mammalian SMC1. *Mol. Cell. Biol.* 21:6984–6998. doi:10.1128/MCB.21.20.6984-6998.2001

Revenkova, E., M. Eijpe, C. Heyting, C.A. Hodges, P.A. Hunt, B. Liebe, H. Scherthan, and R. Jessberger. 2004. Cohesin SMC1 beta is required for meiotic chromosome dynamics, sister chromatid cohesion and DNA recombination. *Nat. Cell Biol.* 6:555–562. doi:10.1038/ncb1135

Riou, L., H. Bastos, B. Lassalle, M. Coureuil, J. Testart, F.D. Boussin, I. Allemand, and P. Fouchet. 2005. The telomerase activity of adult mouse testis resides in the spermatogonial alpha6-integrin-positive side population enriched in germinal stem cells. *Endocrinology.* 146:3926–3932. doi:10.1210/en.2005-0502

Roig, I., B. Liebe, J. Egozcue, L. Cabero, M. Garcia, and H. Scherthan. 2004. Female-specific features of recombinational double-stranded DNA repair in relation to synapsis and telomere dynamics in human oocytes. *Chromosoma.* 113:22–33. doi:10.1007/s00412-004-0290-8

Scherthan, H. 2007. Telomere attachment and clustering during meiosis. *Cell. Mol. Life Sci.* 64:117–124. doi:10.1007/s00018-006-6463-2

Scherthan, H., M. Jerratsch, B. Li, S. Smith, M. Hultén, T. Lock, and T. de Lange. 2000. Mammalian meiotic telomeres: protein composition and redistribution in relation to nuclear pores. *Mol. Biol. Cell.* 11:4189–4203.

Scherthan, H., H. Wang, C. Adelfalk, E.J. White, C. Cowan, W.Z. Cande, and D.B. Kaback. 2007. Chromosome mobility during meiotic prophase in *Saccharomyces cerevisiae*. *Proc. Natl. Acad. Sci. USA.* 104:16934–16939. doi:10.1073/pnas.0704860104

Schmitt, J., R. Benavente, D. Hodzic, C. Höög, C.L. Stewart, and M. Alsheimer. 2007. Transmembrane protein Sun2 is involved in tethering mammalian meiotic telomeres to the nuclear envelope. *Proc. Natl. Acad. Sci. USA.* 104:7426–7431. doi:10.1073/pnas.0609198104

Schotta, G., M. Lachner, K. Sarma, A. Ebert, R. Sengupta, G. Reuter, D. Reinberg, and T. Jenuwein. 2004. A silencing pathway to induce H3-K9 and H4-K20 trimethylation at constitutive heterochromatin. *Genes Dev.* 18:1251–1262. doi:10.1101/gad.300704

Siderakis, M., and M. Tarsounas. 2007. Telomere regulation and function during meiosis. *Chromosome Res.* 15:667–679. doi:10.1007/s10577-007-1149-7

Starling, J.A., J. Maule, N.D. Hastie, and R.C. Allshire. 1990. Extensive telomere repeat arrays in mouse are hypervariable. *Nucleic Acids Res.* 18:6881–6888. doi:10.1093/nar/18.23.6881

Storre, J., A. Schäfer, N. Reichert, J.L. Barbero, S. Hauser, M. Eilers, and S. Gaubatz. 2005. Silencing of the meiotic genes SMC1beta and STAG3 in somatic cells by E2F6. *J. Biol. Chem.* 280:41380–41386. doi:10.1074/jbc.M506797200

Tanemura, K., A. Ogura, C. Cheong, H. Gotoh, K. Matsumoto, E. Sato, Y. Hayashi, H.W. Lee, and T. Kondo. 2005. Dynamic rearrangement of telomeres during spermatogenesis in mice. *Dev. Biol.* 281:196–207. doi:10.1016/j.ydbio.2005.02.025

Vasileva, A., R.M. Linden, and R. Jessberger. 2006. Homologous recombination is required for AAV-mediated gene targeting. *Nucleic Acids Res.* 34:3345–3360. doi:10.1093/nar/gkl455

Vogt, E., M. Kirsch-Volders, J. Parry, and U. Eichenlaub-Ritter. 2008. Spindle formation, chromosome segregation and the spindle checkpoint in mammalian oocytes and susceptibility to meiotic error. *Mutat. Res.* 651:14–29.

Yuan, L., J.G. Liu, J. Zhao, E. Brundell, B. Daneholt, and C. Höög. 2000. The murine SCP3 gene is required for synaptonemal complex assembly, chromosome synapsis, and male fertility. *Mol. Cell.* 5:73–83. doi:10.1016/S1097-2765(00)80404-9